

**UCC Library and UCC researchers have made this item openly available.
Please [let us know](#) how this has helped you. Thanks!**

Title	Wave energy converter configuration in dual wave farms
Author(s)	Bergillos, Rafael J.; Rodriguez-Delgado, Cristobal; Allen, James; Iglesias, Gregorio
Publication date	2019-03-11
Original citation	Bergillos, R. J., Rodriguez-Delgado, C., Allen, J. and Iglesias, G. (2019) 'Wave energy converter configuration in dual wave farms', Ocean Engineering, 178, pp. 204-214. doi: 10.1016/j.oceaneng.2019.03.001
Type of publication	Article (peer-reviewed)
Link to publisher's version	http://www.sciencedirect.com/science/article/pii/S0029801819300939 http://dx.doi.org/10.1016/j.oceaneng.2019.03.001 Access to the full text of the published version may require a subscription.
Rights	© 2019 Elsevier Ltd. All rights reserved. This manuscript version is made available under the CC BY-NC-ND 4.0 licence. https://creativecommons.org/licenses/by-nc-nd/4.0/
Embargo information	Access to this article is restricted until 24 months after publication by request of the publisher.
Embargo lift date	2021-03-11
Item downloaded from	http://hdl.handle.net/10468/9465

Downloaded on 2021-11-27T10:26:52Z

Wave energy converter configuration in dual wave farms

Rafael J. Bergillos^{a,*}, Cristobal Rodriguez-Delgado^{b,c}, James Allen^b, Gregorio Iglesias^{d,b}

^a*Hydraulic Engineering Area, Department of Agronomy, University of Córdoba, Rabanales Campus, Leonardo Da Vinci Building, 14071 Córdoba, Spain*

^b*School of Engineering, University of Plymouth, Plymouth PL4 8AA, UK*

^c*PROES Consultores, Calle San Germán 39, 28020 Madrid, Spain*

^d*MaREI, Environmental Research Institute & School of Engineering, University College Cork, College Road, Cork, Ireland*

Abstract

Wave farms, i.e., arrays of Wave Energy Converters (WECs), have recently been proven to be effective in fulfilling the dual function of carbon-free energy generation and coastal protection. In this paper these dual-function wave farms are referred as dual wave farms. The objective of this work is to investigate the influence of the WEC configuration on the performance of these dual wave farms through a case study: a dual wave farm consisting of WaveCat WECs deployed off an eroding beach. WaveCat is a floating overtopping WEC consisting of two hulls joined by their stern, forming a wedge. Two configurations are considered, with wedge angles of 30° and 60° . To characterize wave-WEC interaction, laboratory tests of a 1:30 WaveCat model are conducted using the two configurations and low-, mid- and high-energy sea states characteristic of the study area. The reflection and transmission coefficients obtained from the laboratory tests are inputted into a suite of numerical models to investigate the hydro- and morphodynamics of the beach. We find that the smaller wedge angle (30°) WECs afford more (less) coastal protection - quantified in terms of dry beach area availability - for short (long) peak periods than WECs with 60° . These results allow us to conclude that, for optimum performance of dual wave farms, WEC geometry should be adapted dynamically to the sea state.

*Corresponding author.

E-mail address: rafael.bergillos@uco.es (R.J. Bergillos)

Keywords: Ocean energy; wave farm; laboratory experiments; numerical modelling; device design

1. Introduction

The development of renewable energy is one of the most relevant targets confronting society in the coming decades [1, 2], due to the finite nature of fossil fuels, their high costs and, last but not least, the environmental impacts of their exploration and use [3, 4]. Among the carbon-free energy sources, marine energy resources offer a vast potential and comparatively low effects on the environment [5–9]. In particular, the worldwide potential of wave energy was assessed as 17 TW h/year [10]. These facts contrast with the low degree of development and utilization of wave energy compared to other renewable sources, such as hydroelectric, biomass or wind energy [11, 12].

For these reasons, increasing research efforts have focused on wave energy over the last years. The objectives of the investigations carried out so far have been: (1) the assessment and characterization of wave energy resources [13–25], (2) the study and optimization of possible locations [26–33], (3) the economic viability of wave energy [34–38], (4) the combined implementation with other ocean energies, most notably, wind [39–44], and (5) the development of wave energy technologies and devices [23, 45–63, 63–75].

One of the wave energy converters (WECs) under development is WaveCat [13, 76]. A floating, overtopping WEC, it comprises two hulls joined at the stern by a hinge – for a detailed description of the device, the reader is referred to [48, 77]. Wave farms consisting of WaveCat WECs have been proven to fulfil a dual function as wave energy generators and coastal defence elements on both sandy beaches [78–81] and gravel-dominated coasts [82–86].

So far, the effects of the WEC configuration on the hydro- and morphodynamics of the coast in the lee of the wave farm have not been studied. The main objective of the present research is to analyse the effects of the configuration of WaveCat, in particular, the wedge angle or angle between the twin hulls, on

28 wave propagation, longshore sediment transport (LST) and shoreline dynamics,
 29 considering the varying transmission and reflection coefficients obtained from
 30 laboratory experiments under different sea states.

31 The laboratory experiments were conducted in the Ocean Basin of the Uni-
 32 versity of Plymouth (Section 3.1). In addition, this research involved the appli-
 33 cation of a wave propagation model (Section 3.2.1), an LST formulation (Sec-
 34 tion 3.2.2) and a one-line model (Section 3.2.3) to a study site in southern Spain
 35 (Section 2).

36 2. Study site

37 Playa Granada is a gravel-dominated deltaic beach located on the Mediter-
 38 ranean coastline of southern Spain (Figure 1a). The beach, which is bounded
 39 by the Guadalfeo River mouth to the west and by *Punta del Santo* to the east
 40 (Figure 1b), has been experiencing shoreline retreat and terminal erosion in re-
 41 cent years [87–89], partly due to anthropogenic interventions in the Guadalfeo
 42 River basin [90–92].

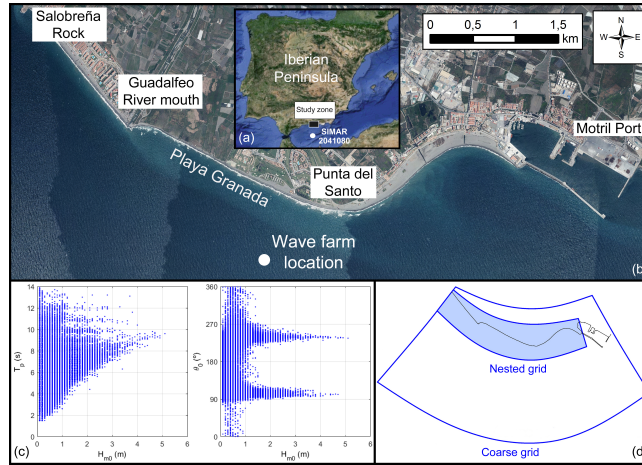


Figure 1: (a) Locations of the study zone and SIMAR point 2041080 in southern Iberian Peninsula. (b) Aerial image of the deltaic coast, indicating the wave farm location and the studied coastline section (Playa Granada). (c) Distributions $H_{m0}-T_p$ and $H_{m0}-\theta_0$ according to the SIMAR data. (d) Computational grids employed to apply the wave propagation model.

43 Two incoming wave directions are predominant at the study site (Figure 1c):
 44 south-west (SW) and south-east (SE). The values of deep-water significant wave
 45 height which are not exceeded 50%, 90%, 99% and 99.9% of the time are 0.5 m,
 46 1.2 m, 2.1 m and 3.1 m, respectively [93]. The astronomical tidal range is ~ 0.6
 47 m [94] and surge levels under storm conditions frequently exceed 0.5 m [95].

48 3. Methods

49 3.1. Laboratory experiments

50 Laboratory tests were performed in the Ocean Basin of the University of
 51 Plymouth to measure the reflection (K_r) and transmission (K_t) coefficients for
 52 two different wedge angles, i.e., angles between the hulls of WaveCat ($\alpha = 30^\circ$
 53 and $\alpha = 60^\circ$, Figure 2). The experiments were carried out at a 1:30 scale and
 54 the dimensions of the model were 3 m (length) and 0.6 m (height) (Figure 2).

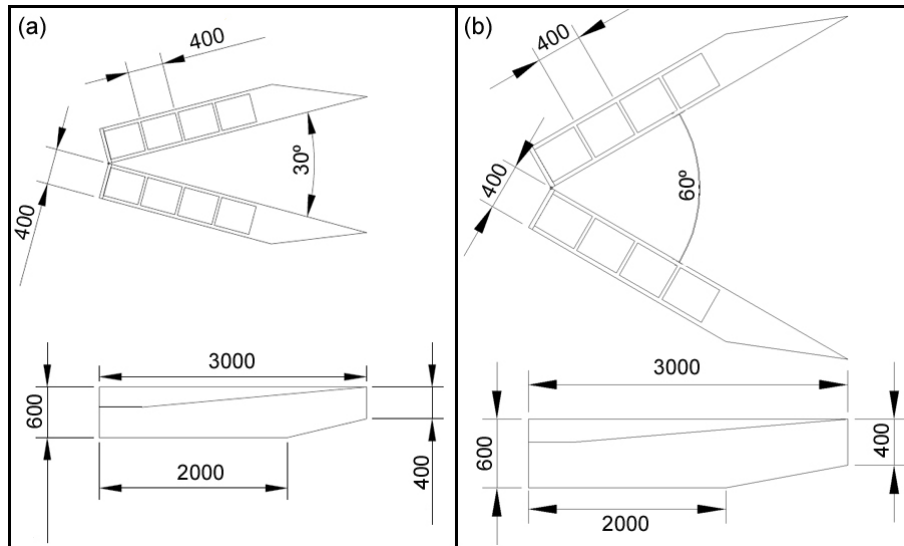


Figure 2: WEC configurations considered, model scale (dimensions in mm): (a) $\alpha = 30^\circ$, (b) $\alpha = 60^\circ$.

55 The selection of the two wedge angle values was done to represent two dif-
56 ferent types of operation of WaveCat corresponding to two different types of
57 sea state: one in which the length of the incoming wave front that is harnessed
58 by the device is maximised ($\alpha = 60^\circ$), given that the wave power per linear
59 metre of wave front is limited (low-energy sea state); and another in which the
60 amount of wave power per linear meter of wave front is substantial (high-energy
61 sea state), and therefore harnessing a shorter stretch of wave front is sufficient
62 to reach the rated power of the device ($\alpha = 30^\circ$).

63 Twelve different sea states were tested, with values of the significant wave
64 height (H_{m0}) between 0.03 m and 0.1 m (1 m and 3 m) in the model (prototype).
65 The tested values of the spectral peak period ($T_{p,mod}$) ranged from 1.28 s to 2.37
66 s, representing real values ($T_{p,prot}$) from 7 s to 13 s (Froude similarity). These
67 sea states are representative of the wave conditions in Playa Granada (Figure
68 1c). The tested sea states, along with the measured reflection and transmission
69 coefficients, are summarized in Table 1. A detailed description of the laboratory
70 experiments can be found in [96, 97].

71 3.2. Numerical modelling

72 3.2.1. SWAN model

73 The SWAN model was used to propagate the sea states in the prototype
74 scale, detailed in Section 3.1, from deep-water toward the coast for the two pre-
75 vailing directions at the study zone (Figure 1c): SW (238°) and SE (107°). The
76 model was previously calibrated for the study area by [98] through comparison
77 with field data.

78 The wave farm location, shown in Figure 1b, was selected based on the
79 results from previous studies, which have demonstrated that it is the best site
80 in terms of wave energy potential [28] and coastal protection [84]. The wave
81 farm layout, consisting of 11 WaveCat WECs spaced by a distance of 180 m
82 and arranged in two rows, was also chosen on the basis of recent works at the
83 study site [83, 85].

Test case	$H_{m0,mod}$	$H_{m0,prot}$ (m)	$T_{p,mod}$ (s)	$T_{p,prot}$ (s)	α ($^{\circ}$)	K_r (-)	K_t (-)
S1_30	0.03	1	1.28	7	30	0.558	0.271
S2_30	0.03	1	1.64	9	30	0.436	0.368
S3_30	0.03	1	2.01	11	30	0.329	0.413
S4_30	0.03	1	2.37	13	30	0.268	0.441
S5_30	0.07	2	1.28	7	30	0.49	0.293
S6_30	0.07	2	1.64	9	30	0.399	0.363
S7_30	0.07	2	2.01	11	30	0.326	0.414
S8_30	0.07	2	2.37	13	30	0.266	0.439
S9_30	0.1	3	1.28	7	30	0.428	0.304
S10_30	0.1	3	1.64	9	30	0.361	0.359
S11_30	0.1	3	2.01	11	30	0.322	0.415
S12_30	0.1	3	2.37	13	30	0.265	0.437
S1_60	0.03	1	1.28	7	60	0.726	0.28
S2_60	0.03	1	1.64	9	60	0.499	0.359
S3_60	0.03	1	2.01	11	60	0.277	0.381
S4_60	0.03	1	2.37	13	60	0.213	0.387
S5_60	0.07	2	1.28	7	60	0.627	0.274
S6_60	0.07	2	1.64	9	60	0.351	0.342
S7_60	0.07	2	2.01	11	60	0.254	0.382
S8_60	0.07	2	2.37	13	60	0.186	0.399
S9_60	0.1	3	1.28	7	60	0.567	0.269
S10_60	0.1	3	1.64	9	60	0.399	0.336
S11_60	0.1	3	2.01	11	60	0.262	0.375
S12_60	0.1	3	2.37	13	60	0.189	0.396

Table 1: Wave conditions in the model ($H_{m0,mod}$, $T_{p,mod}$) and prototype ($H_{m0,prot}$, $T_{p,prot}$) scales, angle between hulls (α), reflection coefficient (K_r) and transmission coefficient (K_t) of the cases tested in the laboratory.

84 Two numerical grids were defined and used (Figure 1d): a coarse grid cov-
85 ering the entire deltaic region and extending from deep to shallow waters, and
86 a nested grid covering the nearshore region, including the wave farm area, with
87 higher resolution. To properly model the wave farm effects, the WECs were
88 introduced in SWAN as artificial obstacles, specifying their reflection and trans-
89 mission coefficients (hereafter denoted by K_r and K_t , respectively) for each sea
90 state and wedge angle (Table 1). The results provided by SWAN were utilized
91 to obtain wave variables at breaking conditions (through the fraction breaking
92 variable) and, on this basis, apply the LST formulation below.

93 *3.2.2. Longshore sediment transport formulation*

94 LST was obtained through the formulation proposed by [99], which was
95 found in previous work [98] to provide good estimates of the measured LST
96 rates at the study site. The following expression was used:

$$Q = 0.00018K\rho_s g^{0.5} (\tan \beta)^{0.4} (d_{50})^{-0.6} (H_{m,br})^{3.1} \sin(2\theta_{br}), \quad (1)$$

97 where Q is the LST rate, ρ_s is the sediment density, g the gravity accelera-
98 tion, $\tan \beta$ the beach slope of the surf zone, d_{50} the grain size, $H_{m,br}$ (θ_{br}) the
99 breaking significant wave height (wave angle respect to shore-normal) and the
100 coefficient K considers the effect of wave period on LST.

101 *3.2.3. One-line model*

102 The LST rates obtained with the equation of [99] and detailed in the previous
103 section were used to calculate the changes in the shoreline position through the
104 application of a one-line model [100], which is based on the following equation:

$$\frac{\partial y_s}{\partial t} = -\frac{1}{D} \left(\frac{\partial Q}{\partial x_s} \right), \quad (2)$$

105 where y_s and x_s are the coordinates of the shoreline, t is the time, and D
106 is the sum of the height of the berm and the closure depth. [98] proved that
107 the joint application of the SWAN model, the LST formulation of [99] and the
108 one-line model replicates the coastline changes in Playa Granada.

109 **4. Results**

110 *4.1. Significant wave heights at breaking*

111 This section details the influence of the wave farm on wave propagation – in
112 particular, on the significant wave heights at breaking – depending on the wedge
113 of the WECs. The alongshore variation of the differences between breaking
114 significant wave heights for $\alpha = 30^\circ$ and $\alpha = 60^\circ$ ($\Delta H_{m,br}$) are indicated in
115 Figure 3.

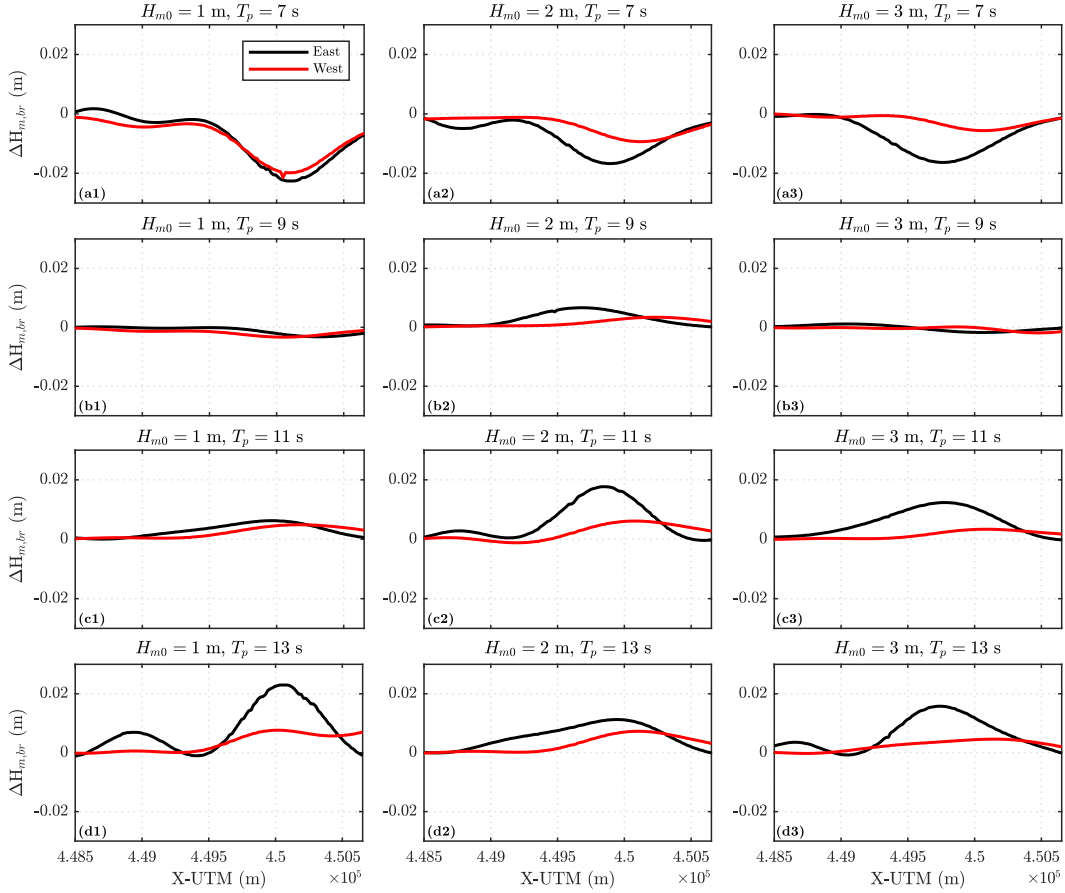


Figure 3: Alongshore distribution of the differences between the significant wave heights at breaking for $\alpha = 30^\circ$ and $\alpha = 60^\circ$ under SW (red) and SE (black) waves. $[\Delta H_{m,br} = H_{m,br,30} - H_{m,br,60}]$.

116 Under SW waves, it is shown that the differences are generally negative for
 117 short wave periods ($T_p = 7$ s) and positive for long periods ($T_p = 11$ s and
 118 $T_p = 13$ s). In all the cases, the maximum differences are reached at the eastern
 119 part of the coast, influenced by the location of the wave farm (shown in Figure
 120 1) and its effects in the leeward wave propagation patterns.

121 For all the H_{m0} , the alongshore-averaged values of $\Delta H_{m,br}$ for SW waves
 122 increase with increasing values of T_p (Figure 4). Thus, in terms of wave energy
 123 at the breaking zone, the wave farm composed by devices with the 30° config-

124 uration provides more (less) protection for short (long) T_p than that with the
 125 60° configuration. This is a result of the different K_r and K_t of both configura-
 126 tions (Table 1). For given values of T_p , the differences in breaking wave heights
 127 between both angles decrease for increasing values of H_{m0} (Figure 4).

128 Under incoming SE waves, the differences are also negative (positive) for
 129 short (long) T_p , although in this case they extend along most of the study stretch
 130 (Figure 3). For constant values of H_{m0} , the alongshore-averaged $\Delta H_{m,br}$ under
 131 SE waves is greater for longer T_p (Figure 4); it is also due to the differences in
 132 K_r and K_t between both devices (Table 1). Thus, the greater the values of T_p ,
 133 the lower the protection provided by devices with $\alpha = 30^\circ$ compared to those
 134 with $\alpha = 60^\circ$.

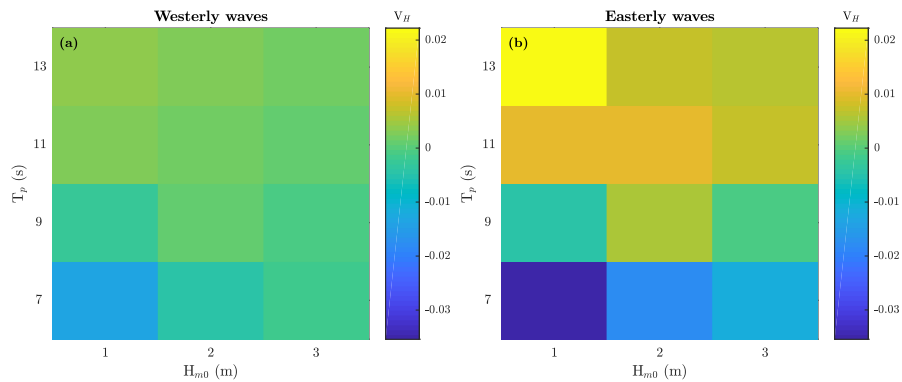


Figure 4: Variation in the alongshore-averaged significant wave heights at breaking for $\alpha = 30^\circ$ with respect to the values for $\alpha = 60^\circ$ under SW (a) and SE (b) waves. [$V_H = (\bar{H}_{m,br,30} - \bar{H}_{m,br,60})/\bar{H}_{m,br,30}$].

135 The differences in significant wave height at breaking between both devices
 136 under SE wave conditions are generally greater than those under SW waves
 137 (Figure 4); with maximum negative (positive) alongshore-averaged values of
 138 $\Delta H_{m,br}$ equal to -0.82 cm (0.77 cm) for low-energy waves ($H_{m0}=1$ m), -0.77
 139 cm (0.55 cm) for mid-energy waves ($H_{m0}=2$ m), and -0.71 cm (0.61 cm) for
 140 high-energy waves ($H_{m0}=3$ m).

141 4.2. Longshore sediment transport rates

142 The differences in LST rates between the WECs with $\alpha = 30^\circ$ and $\alpha = 60^\circ$
 143 are analysed in this section. Figure 5 depicts the alongshore distribution of these
 144 differences for all the sea states considered. Under SW waves, the differences
 145 are generally greater for higher values of $H_{m,0}$ and lower values of T_p , i.e. the
 146 greater the wave steepness, the higher the differences in LST rates between the
 147 farms with both angles. The differences are more significant in the western
 148 (eastern) stretch of the coast for short (long) peak periods (Figure 5).

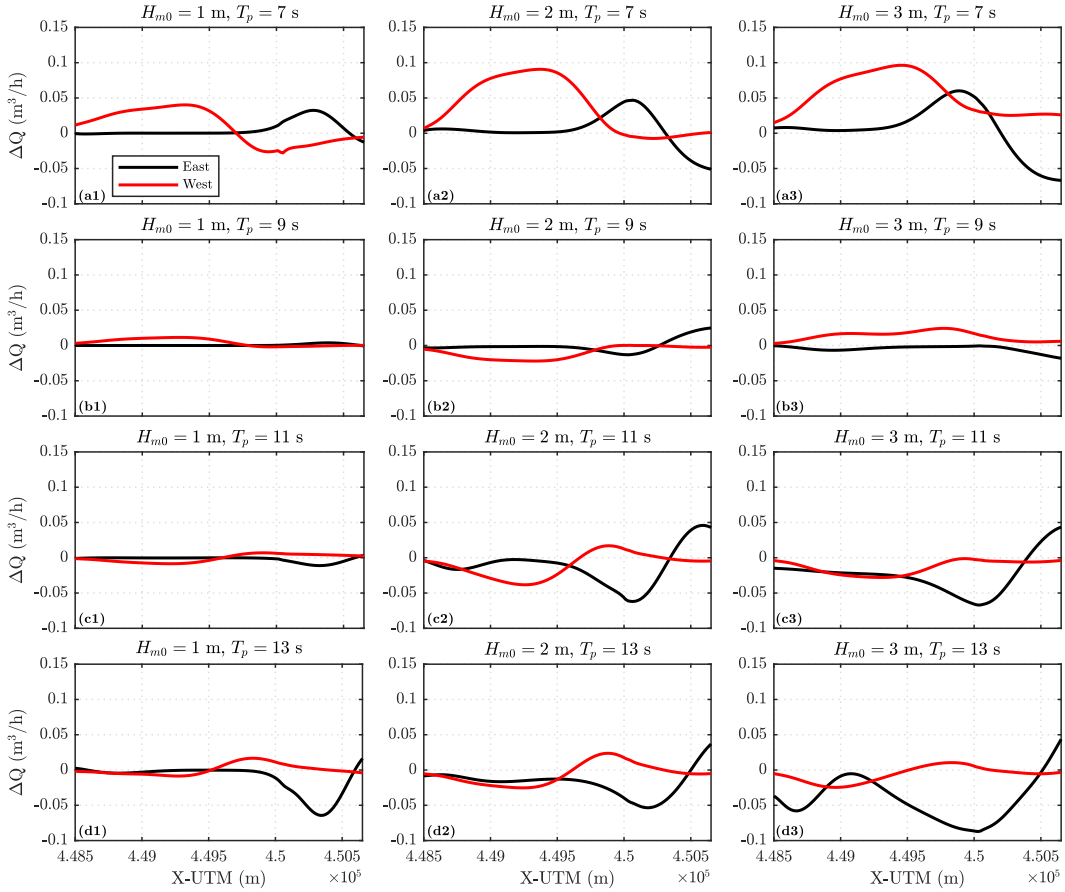


Figure 5: Alongshore distribution of the differences between the LST rates for $\alpha = 30^\circ$ and $\alpha = 60^\circ$ under SW (red) and SE (black) waves. $[\Delta Q = Q_{30} - Q_{60}]$.

149 Under SE wave conditions, the greater differences are located in the eastern

150 part of the study section (Figure 5), i.e., in the lee of the wave farm (Figure 1).
 151 For short periods ($T_p = 7$ s), the differences are negative in the eastern end of
 152 the stretch of beach and become positive toward the west; whereas the opposite
 153 occurs for long periods ($T_p = 11$ s and $T_p = 13$ s). In general, the differences
 154 are greater as the $H_{m,0}$ values increase (Table 2).

	SW waves			SE waves		
	$H_{m,0}=1$ m	$H_{m,0}=2$ m	$H_{m,0}=3$ m	$H_{m,0}=1$ m	$H_{m,0}=2$ m	$H_{m,0}=3$ m
$T_p=7$ s	-0.0092	-0.0385	-0.0548	-0.0055	-0.0052	-0.0073
$T_p=9$ s	-0.0045	0.0105	-0.0136	-0.0006	0.001	0.0044
$T_p=11$ s	0.0006	0.0104	0.0134	0.002	0.0128	0.0256
$T_p=13$ s	-0.0007	0.0054	0.0062	0.0116	0.0185	0.0425

Table 2: Differences between the alongshore-averaged LST rates for $\alpha = 30^\circ$ and $\alpha = 60^\circ$ under SW and SE waves (in m^3/h).

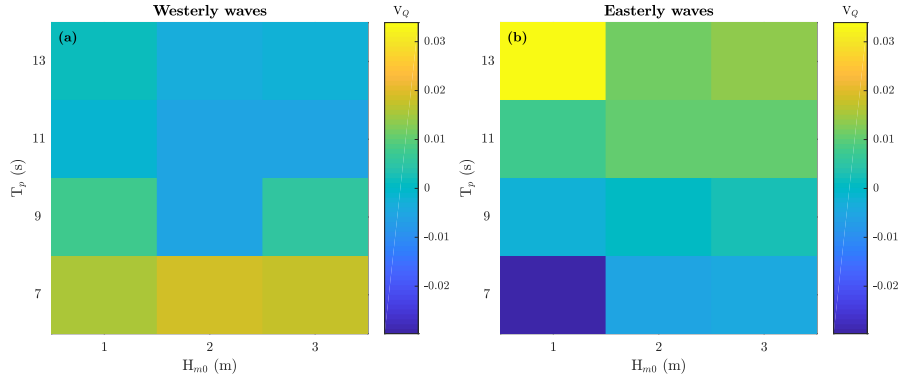


Figure 6: Variation in the alongshore-averaged LST rates for $\alpha = 30^\circ$ with respect to the values for $\alpha = 60^\circ$ under SW (a) and SE (b) waves. $[V_Q = (\bar{Q}_{30} - \bar{Q}_{60})/\bar{Q}_{30}]$.

155 The differences in LST rates between the farms composed by both devices
 156 under SE wave conditions are greater than those under SW waves (Table 2
 157 and Figure 6). This is influenced by both the higher differences in breaking
 158 significant wave heights (Section 4.1) and the higher angles from shore-normal
 159 for SE waves, which increase the LST rates and differences.

160 4.3. Shoreline geometry

161 The LST rates obtained in the previous section were used to compute the
 162 variations in the shoreline morphology over a one-month period for $H_{m,0}=1$ m,
 163 $H_{m,0}=2$ m and $H_{m,0}=3$ m, representing low-, mid- and high-energy conditions,
 164 respectively. The differences between the final shorelines for $\alpha = 30^\circ$ and $\alpha =$
 165 60° under both SW and SE waves are shown in Figure 7.

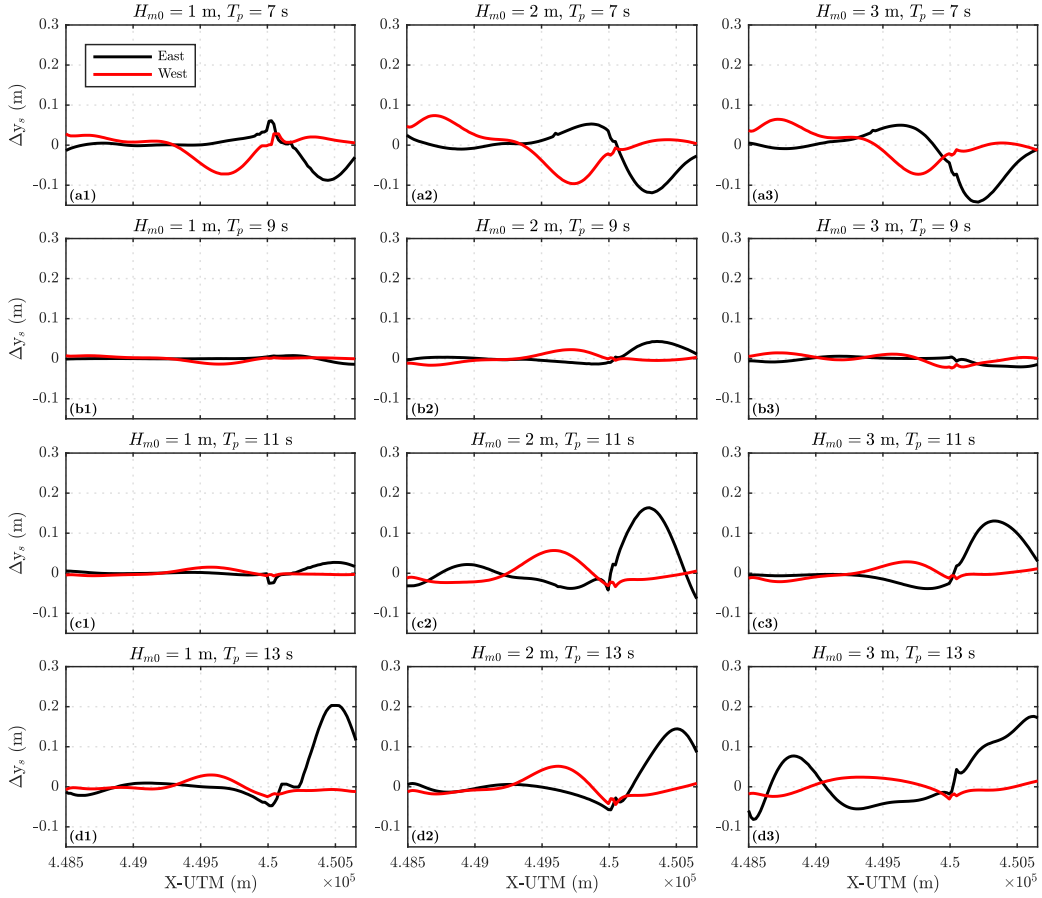


Figure 7: Alongshore distribution of the the differences between the final coastline positions (after 1 month) for $\alpha = 30^\circ$ and $\alpha = 60^\circ$ under SW (red) and SE (black) waves. [$\Delta y = y_{\text{final},30} - y_{\text{final},60}$].

166 For SW waves and short peak periods ($T_p=7$ s), the maximum differences
 167 are negative and concentrated in the central stretch of beach (where the main

168 occupations are located), indicating that the wave farm with $\alpha = 30^\circ$ provides
 169 greater protection at this location. On the contrary, the differences in the west-
 170 ern part of the beach are positive (Figure 7), i.e., the farm with $\alpha = 60^\circ$ leads
 171 to greater accretion near the river mouth for short wave periods. This section
 172 has experienced acute shoreline retreat in recent years due to river damming
 173 [91].

174 For long wave periods ($T_p=11$ s and $T_p=13$ s), the maximum differences
 175 under SW waves are positive and located in the central stretch of beach. In
 176 addition, the alongshore-averaged values are positive for low-, mid- and high-
 177 energy conditions (Table 3). Thus, under SW waves with long periods, the wave
 178 farm with $\alpha = 60^\circ$ provides greater protection against shoreline erosion. This
 179 leads to a higher efficiency in terms of dry beach area (Section 4.4).

	SW waves			SE waves		
	$H_{m0}=1$ m	$H_{m0}=2$ m	$H_{m0}=3$ m	$H_{m0}=1$ m	$H_{m0}=2$ m	$H_{m0}=3$ m
$T_p=7$ s	-0.36	-0.06	0.21	-0.66	-1.06	- 1.65
$T_p=9$ s	-0.04	-0.04	0.02	0.01	0.54	0.39
$T_p=11$ s	0.05	0.05	0.01	0.3	1.65	1.48
$T_p=13$ s	0.1	0.06	0.03	2.1	1.23	2.01

Table 3: Differences between the alongshore-averaged final coastline positions for $\alpha = 30^\circ$ and $\alpha = 60^\circ$ under SW and SE waves (in cm).

180 On the other hand, under SE waves, the greatest differences are concentrated
 181 along the eastern section of the coastline. This is caused by the farm location
 182 (Figure 1) and the resulting greater differences in LST between both angles at
 183 this stretch of beach (Figure 5). The differences in final shoreline positions are
 184 generally negative (positive) for short (long) peak periods, indicating that the
 185 wave farm composed by WECs with $\alpha = 30^\circ$ ($\alpha = 60^\circ$) provides more protection
 186 for short (long) wave periods (Figure 5 and Table 3).

187 For all the sea states considered, the differences in the final shoreline geome-
 188 tries between devices with $\alpha = 30^\circ$ and $\alpha = 60^\circ$ under SE wave conditions are
 189 higher than those under SW waves. These differences determine the dry beach
 190 area availability, as explained in the following section.

191 4.4. Dry beach area

192 The differences between the final and initial dry beach areas for all the sea
 193 states analysed and for both angles between the hulls are depicted in Figure 8. It
 194 may be observed that these differences are always positive, i.e., beach accretion
 195 occurs in all cases. This confirms the efficiency of wave farms as protection
 196 elements against coastline erosion.

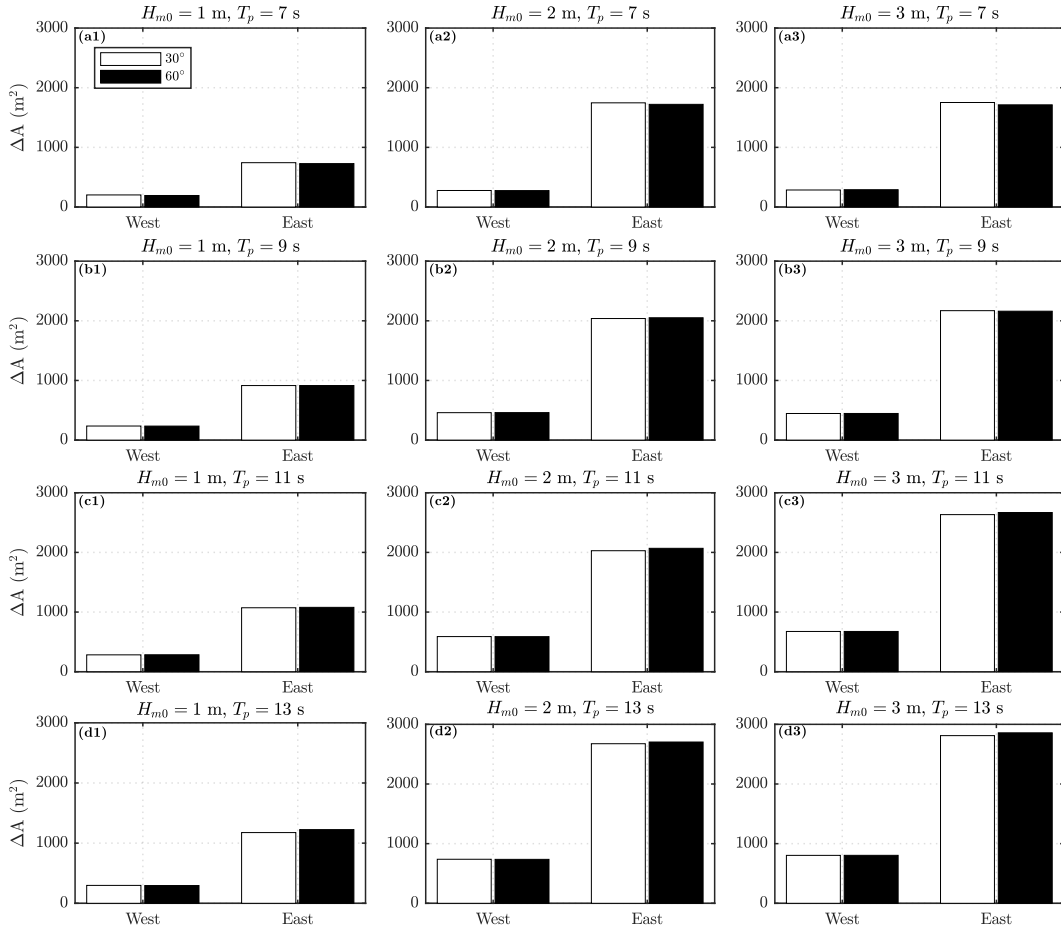


Figure 8: Dry beach area variations for $\alpha = 30^\circ$ (white) and $\alpha = 60^\circ$ (black) under SW and SE waves. [$\Delta A = A_{\text{final}} - A_{\text{initial}}$].

197 As shown in Figure 8, the accretion is more pronounced under SE waves.
 198 This is in agreement with the observed morphological response of the coastline,
 199 since SW waves contribute to erode the beach and SE waves lead to beach recovery
 200 [98, 101]. In this case, the presence of the farm increases the beach accretion
 201 under SE waves and reverts the coastline response (from erosion to accretion)
 202 under SW wave conditions. The dry beach area differences are generally greater
 203 with increasing values of H_{m0} and T_p (Figure 8).

204 The comparison of the results obtained for both angles between hulls allow
 205 concluding that, under SW waves, the farm composed by devices with $\alpha = 60^\circ$
 206 is more efficient in terms of coastal protection for all the cases except four of
 207 them (associated to mild conditions): $H_{m0}=1$ m - $T_p=7$ s, $H_{m0}=1$ m - $T_p=9$
 208 s, $H_{m0}=2$ m - $T_p=7$ s and $H_{m0}=2$ m - $T_p=9$ s (Table 4 and Figure 9). Under
 209 SE waves, the WaveCat devices with $\alpha = 30^\circ$ are more efficient for the shortest
 210 peak period ($T_p=7$ s), whereas those with $\alpha = 60^\circ$ lead to greater accretion
 211 values for the rest of wave conditions (Table 4).

	SW waves			SE waves		
	$H_{m0}=1$ m	$H_{m0}=2$ m	$H_{m0}=3$ m	$H_{m0}=1$ m	$H_{m0}=2$ m	$H_{m0}=3$ m
$T_p=7$ s	9.4	1.8	-4.7	15.4	26	39
$T_p=9$ s	1	0.9	-0.5	-0.5	-13	-9
$T_p=11$ s	-1.3	-1.1	-0.1	-7	-41	-36
$T_p=13$ s	-2.3	-1.4	-0.7	-49	-29	-47

Table 4: Differences between the final dry beach area for $\alpha = 30^\circ$ and $\alpha = 60^\circ$ under SW and SE waves (in m^2).

212 The results of this section indicate that, for the best performance in terms of
 213 coastal protection, the geometry of the WECs should be adjusted dynamically
 214 to the sea state. If this is not possible, i.e., if a fixed configuration (constant
 215 wedge angle) must be adopted, then this configuration should be chosen on the
 216 basis of a detailed analysis of the wave climate at the site of interest, with a
 217 view to optimizing the coastal protection performance under the prevailing sea
 218 states.

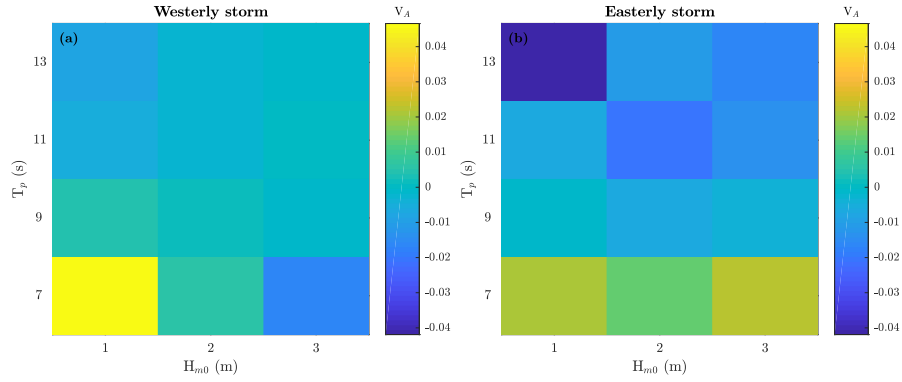


Figure 9: Variation in the dry beach area differences for $\alpha = 30^\circ$ with respect to the values for $\alpha = 60^\circ$ under SW (a) and SE (b) waves. $[V_A = (\Delta A_{30} - \Delta A_{60})/\Delta A_{30}]$.

219 The methodology presented in this work, which combines laboratory tests
 220 with different WEC configurations and numerical modelling, may be used for
 221 other geometries and beaches to investigate the optimum configuration for a
 222 wave farm project.

223 5. Conclusions

224 Wave energy is one of the renewables with the greatest potential for develop-
 225 ment due to the resource availability and low visual pollution. Recent research
 226 has highlighted the possibility of using wave farms for a dual function, i.e.,
 227 renewable energy generation and coastal protection.

228 This paper presents the first study on the influence of WEC configuration
 229 on the performance of dual wave farms. In particular, the effects of two values
 230 of the wedge angle, i.e., the angle between the twin hulls of WaveCat WECs
 231 ($\alpha = 30^\circ$ and $\alpha = 60^\circ$) on significant wave height at breaking, LST rates,
 232 shoreline geometry and dry beach area were analysed. For this purpose, the
 233 transmission and reflection coefficients were determined for relevant sea states
 234 based on laboratory experiments in a wave tank, and these values were used to
 235 model the wave farm-induced morphological variations on a gravel-dominated
 236 beach.

237 The results indicate that, under both SW and SE waves, the wave farm
238 composed by WaveCat devices with $\alpha = 30^\circ$ provides more (less) protection for
239 short (long) peak periods, quantified in terms of breaking wave heights. This
240 is down to the different values of the transmission and reflection coefficients
241 corresponding to the two configurations. The differences in significant wave
242 height at breaking between the two WEC configurations under SE waves are
243 generally greater than those under SW waves. This, along with the more oblique
244 incidence for SE waves, leads to greater differences in LST rates between the
245 two configurations under SE waves.

246 The LST rates thus obtained were used to compute the changes in shoreline
247 geometry and dry beach area. The results confirm the efficiency of wave farms in
248 coastal protection indeed, accretion occurs under all the sea states considered.
249 The gains in dry beach area obtained with the 60° WEC configuration were
250 generally greater for long peak periods ($T_p=11$ s and $T_p=13$ s) and lower for
251 the shortest peak period ($T_p=7$ s). We conclude that the performance of dual
252 wave farms depends on both the WEC configuration and the sea state. In other
253 words, the optimum configuration depends on the sea state.

254 Therefore, for maximum performance of the wave farm in coastal erosion
255 protection, the WEC geometry should be adjusted dynamically to the sea state.
256 This dynamic adaptation strategy leads to a greater dry beach area. With
257 the methodology presented in this paper, this benefit may be quantified for
258 any beach of interest, and compared with the cost of the dynamic adaptation
259 strategy versus a constant geometry strategy in order to establish which is more
260 appropriate. Future research should focus on the assessment of the role of WEC
261 configuration in power production, investigating the optimum pair angle-draft
262 that maximises power production.

263 **Acknowledgements**

264 This paper was carried out in the framework of research grants WAVEIM-
265 PACT (PCIG-13-GA-2013-618556, European Commission, Marie Curie fellow-
266 ship, fellow GI) and ICE (Intelligent Community Energy, European Commision,
267 Contract no. 5025). RB was funded by the Spanish Ministry of Science, Inno-
268 vation and Universities (*Programa Juan de la Cierva 2017*, FJCI-2017-31781).
269 Wave and bathymetric data were provided by *Puertos del Estado* (Spain) and
270 the Spanish Ministry of Agriculture, Fisheries and Food, respectively. We thank
271 two anonymous reviewers for their improvements to this work.

272 **References**

- 273 [1] European Commission, A European Strategic Energy Technology Plan
274 (Set-Plan): Towards a low carbon future, Brussels: Commission of the
275 European Communities (2007).
- 276 [2] European Commission, Renewable Energy Directive 2009/28/EC , Euro-
277 pean Union, 2009.
- 278 [3] M. Asif, T. Muneer, Energy supply, its demand and security issues for
279 developed and emerging economies, *Renewable and Sustainable Energy*
280 *Reviews* 11 (2007) 1388–1413.
- 281 [4] S. Shafiee, E. Topal, When will fossil fuel reserves be diminished?, *Energy*
282 *policy* 37 (2009) 181–189.
- 283 [5] J. Falnes, A review of wave-energy extraction, *Marine Structures* 20
284 (2007) 185–201.
- 285 [6] A. M. Cornett, A global wave energy resource assessment, in: *The Eigh-*
286 *teenth International Offshore and Polar Engineering Conference*, Interna-
287 *tional Society of Offshore and Polar Engineers*, 2008.
- 288 [7] J. Cruz, *Ocean wave energy: current status and future perspectives*,
289 Springer Science & Business Media, 2008.

- 290 [8] N. Panwar, S. Kaushik, S. Kothari, Role of renewable energy sources in
291 environmental protection: a review, *Renewable and Sustainable Energy*
292 *Reviews* 15 (2011) 1513–1524.
- 293 [9] G. Rinaldi, P. Thies, R. Walker, L. Johanning, A decision support model
294 to optimise the operation and maintenance strategies of an offshore re-
295 newable energy farm, *Ocean Engineering* 145 (2017) 250–262.
- 296 [10] H. Lund, Renewable energy strategies for sustainable development, *En-*
297 *ergy* 32 (2007) 912–919.
- 298 [11] U. E. I. Administration, et al., *Annual Energy Outlook 2011: With Pro-*
299 *jections to 2035*, Government Printing Office, 2011.
- 300 [12] Eurostat, *Renewable energy statistics*, European Union, 2016.
- 301 [13] G. Iglesias, R. Carballo, A. Castro, B. Fraga, Development and design of
302 the WaveCatTM energy converter, in: *Coastal Engineering 2008: (In 5*
303 *Volumes)*, World Scientific, 2009, pp. 3970–3982.
- 304 [14] G. Iglesias, R. Carballo, Choosing the site for the first wave farm in a
305 region: A case study in the Galician Southwest (Spain), *Energy* 36 (2011)
306 5525–5531.
- 307 [15] D. Vicinanza, P. Contestabile, V. Ferrante, Wave energy potential in the
308 north-west of Sardinia (Italy), *Renewable Energy* 50 (2013) 506–521.
- 309 [16] R. Carballo, M. Sánchez, V. Ramos, J. Fraguera, G. Iglesias, The intra-
310 annual variability in the performance of wave energy converters: A com-
311 parative study in N Galicia (Spain), *Energy* 82 (2015) 138 – 146.
- 312 [17] P. Contestabile, V. Ferrante, D. Vicinanza, Wave energy resource along
313 the coast of Santa Catarina (Brazil), *Energies* 8 (2015) 14219–14243.
- 314 [18] M. López, M. Veigas, G. Iglesias, On the wave energy resource of Peru,
315 *Energy Conversion and Management* 90 (2015) 34 – 40.

- 316 [19] D. Silva, A. R. Bento, P. Martinho, C. G. Soares, High resolution local
317 wave energy modelling in the Iberian Peninsula, *Energy* 91 (2015) 1099–
318 1112.
- 319 [20] M. Veigas, M. López, G. Iglesias, Assessing the optimal location for a
320 shoreline wave energy converter, *Applied Energy* 132 (2014) 404 – 411.
- 321 [21] M. Veigas, M. López, P. Romillo, R. Carballo, A. Castro, G. Iglesias,
322 A proposed wave farm on the galician coast, *Energy Conversion and*
323 *Management* 99 (2015) 102–111.
- 324 [22] C. Iuppa, L. Cavallaro, D. Vicinanza, E. Foti, Investigation of suitable
325 sites for Wave Energy Converters around Sicily (Italy)., *Ocean Science*
326 *Discussions* 12 (2015).
- 327 [23] A. Viviano, S. Naty, E. Foti, T. Bruce, W. Allsop, D. Vicinanza, Large-
328 scale experiments on the behaviour of a generalised oscillating water col-
329 umn under random waves, *Renewable Energy* 99 (2016) 875 – 887.
- 330 [24] R. Carballo, N. Arean, M. Álvarez, I. López, A. Castro, M. López, G. Igle-
331 sias, Wave farm planning through high-resolution resource and perfor-
332 mance characterization, *Renewable Energy* (2018).
- 333 [25] L. F. Prieto, G. R. Rodríguez, J. S. Rodríguez, Wave energy to power a
334 desalination plant in the north of Gran Canaria Island: Wave resource,
335 socioeconomic and environmental assessment, *Journal of Environmental*
336 *Management* 231 (2019) 546–551.
- 337 [26] R. Carballo, M. Sánchez, V. Ramos, F. Taveira-Pinto, G. Iglesias, A high
338 resolution geospatial database for wave energy exploitation, *Energy* 68
339 (2014) 572 – 583.
- 340 [27] C. Iuppa, L. Cavallaro, E. Foti, D. Vicinanza, Potential wave energy
341 production by different wave energy converters around Sicily, *Journal of*
342 *Renewable and Sustainable Energy* 7 (2015) 061701.

- 343 [28] A. López-Ruiz, R. J. Bergillos, M. Ortega-Sánchez, The importance of
344 wave climate forecasting on the decision-making process for nearshore
345 wave energy exploitation, *Applied Energy* 182 (2016) 191 – 203.
- 346 [29] N. Elginöz, B. Bas, Life Cycle Assessment of a multi-use offshore platform:
347 Combining wind and wave energy production, *Ocean Engineering* 145
348 (2017) 430–443.
- 349 [30] I. Alifdini, N. A. P. Iskandar, A. W. Nugraha, D. N. Sugianto,
350 A. Wirasatriya, A. B. Widodo, Analysis of ocean waves in 3 sites potential
351 areas for renewable energy development in Indonesia, *Ocean Engineering*
352 165 (2018) 34–42.
- 353 [31] D. Khojasteh, S. M. Mousavi, W. Glamore, G. Iglesias, Wave energy
354 status in asia, *Ocean Engineering* 169 (2018) 344–358.
- 355 [32] A. López-Ruiz, R. J. Bergillos, A. Lira-Loarca, M. Ortega-Sánchez, A
356 methodology for the long-term simulation and uncertainty analysis of the
357 operational lifetime performance of wave energy converter arrays, *Energy*
358 153 (2018) 126–135.
- 359 [33] A. López-Ruiz, R. J. Bergillos, J. M. Raffo-Caballero, M. Ortega-Sánchez,
360 Towards an optimum design of wave energy converter arrays through an
361 integrated approach of life cycle performance and operational capacity,
362 *Applied Energy* 209 (2018) 20 – 32.
- 363 [34] S. Astariz, G. Iglesias, The economics of wave energy: A review, *Renew-
364 able and Sustainable Energy Reviews* 45 (2015) 397 – 408.
- 365 [35] S. Astariz, A. Vazquez, G. Iglesias, Evaluation and comparison of the lev-
366 elized cost of tidal, wave, and offshore wind energy, *Journal of Renewable
367 and Sustainable Energy* 7 (2015) 053112.
- 368 [36] S. Astariz, G. Iglesias, Wave energy vs. other energy sources: A reassess-
369 ment of the economics, *International Journal of Green Energy* 13 (2016)
370 747–755.

- 371 [37] P. Contestabile, E. Di Lauro, M. Buccino, D. Vicinanza, Economic As-
372 sessment of Overtopping Breakwater for Energy Conversion (OBREC):
373 A Case Study in Western Australia, *Sustainability* 9 (2017) 51.
- 374 [38] C. Frost, D. Findlay, E. Macpherson, P. Sayer, L. Johanning, A model to
375 map levelised cost of energy for wave energy projects, *Ocean Engineering*
376 149 (2018) 438–451.
- 377 [39] A. Azzellino, V. Ferrante, J. P. Kofoed, C. Lanfredi, D. Vicinanza, Opti-
378 mal siting of offshore wind-power combined with wave energy through a
379 marine spatial planning approach, *International Journal of Marine Energy*
380 3 (2013) e11–e25.
- 381 [40] S. Astariz, G. Iglesias, Enhancing wave energy competitiveness through
382 co-located wind and wave energy farms. a review on the shadow effect,
383 *Energies* 8 (2015) 7344–7366.
- 384 [41] S. Astariz, J. Abanades, C. Perez-Collazo, G. Iglesias, Improving wind
385 farm accessibility for operation and maintenance through a co-located
386 wave farm: Influence of layout and wave climate, *Energy Conversion and*
387 *Management* 95 (2015) 229 – 241.
- 388 [42] S. Astariz, G. Iglesias, Output power smoothing and reduced downtime
389 period by combined wind and wave energy farms, *Energy* 97 (2016) 69 –
390 81.
- 391 [43] C. Pérez-Collazo, D. Greaves, G. Iglesias, A review of combined wave
392 and offshore wind energy, *Renewable and Sustainable Energy Reviews* 42
393 (2015) 141 – 153.
- 394 [44] Z. Wang, C. Duan, S. Dong, Long-term wind and wave energy resource
395 assessment in the South China sea based on 30-year hindcast data, *Ocean*
396 *Engineering* 163 (2018) 58–75.

- 397 [45] D. Vicinanza, L. Margheritini, J. P. Kofoed, M. Buccino, The SSG wave
398 energy converter: Performance, status and recent developments, *Energies*
399 5 (2012) 193–226.
- 400 [46] A. F. de O. Falcão, Modelling and control of oscillating-body wave energy
401 converters with hydraulic power take-off and gas accumulator, *Ocean*
402 *Engineering* 34 (2007) 2021–2032.
- 403 [47] L. Margheritini, D. Vicinanza, P. Frigaard, SSG wave energy converter:
404 Design, reliability and hydraulic performance of an innovative overtopping
405 device, *Renewable Energy* 34 (2009) 1371–1380.
- 406 [48] H. Fernandez, G. Iglesias, R. Carballo, A. Castro, J. Fraguera, F. Taveira-
407 Pinto, M. Sanchez, The new wave energy converter WaveCat: Concept
408 and laboratory tests, *Marine Structures* 29 (2012) 58–70.
- 409 [49] D. Vicinanza, J. H. Nørgaard, P. Contestabile, T. L. Andersen, Wave
410 loadings acting on overtopping breakwater for energy conversion, *Journal*
411 *of Coastal Research* 65 (2013) 1669–1674.
- 412 [50] I. López, B. Pereiras, F. Castro, G. Iglesias, Optimisation of turbine-
413 induced damping for an OWC wave energy converter using a RANS–VOF
414 numerical model, *Applied Energy* 127 (2014) 105 – 114.
- 415 [51] I. López, G. Iglesias, Efficiency of OWC wave energy converters: A virtual
416 laboratory, *Applied Ocean Research* 44 (2014) 63 – 70.
- 417 [52] D. Vicinanza, P. Contestabile, J. Q. H. Nørgaard, T. L. Andersen, Inno-
418 vative rubble mound breakwaters for overtopping wave energy conversion,
419 *Coastal Engineering* 88 (2014) 154–170.
- 420 [53] A. Day, A. Babarit, A. Fontaine, Y.-P. He, M. Kraskowski, M. Murai,
421 I. Penesis, F. Salvatore, H.-K. Shin, Hydrodynamic modelling of marine
422 renewable energy devices: A state of the art review, *Ocean Engineering*
423 108 (2015) 46–69.

- 424 [54] I. López, B. Pereiras, F. Castro, G. Iglesias, Performance of OWC wave en-
425 ergy converters: Influence of turbine damping and tidal variability, Inter-
426 national Journal of Energy Research 39 (2015) 472–483. ER-13-4164.R2.
- 427 [55] I. López, A. Castro, G. Iglesias, Hydrodynamic performance of an oscil-
428 lating water column wave energy converter by means of particle imaging
429 velocimetry, Energy 83 (2015) 89 – 103.
- 430 [56] I. López, B. Pereiras, F. Castro, G. Iglesias, Holistic performance analysis
431 and turbine-induced damping for an owc wave energy converter, Renew-
432 able Energy 85 (2016) 1155–1163.
- 433 [57] M. Buccino, D. Stagonas, D. Vicinanza, Development of a composite sea
434 wall wave energy converter system, Renewable Energy 81 (2015) 509–522.
- 435 [58] P. Contestabile, C. Iuppa, E. Di Lauro, L. Cavallaro, T. L. Andersen,
436 D. Vicinanza, Wave loadings acting on innovative rubble mound break-
437 water for overtopping wave energy conversion, Coastal Engineering 122
438 (2017) 60–74.
- 439 [59] A. Elhanafi, G. Macfarlane, A. Fleming, Z. Leong, Experimental and
440 numerical investigations on the hydrodynamic performance of a floating-
441 moored oscillating water column wave energy converter, Applied Energy
442 205 (2017) 369 – 390.
- 443 [60] M. López, F. Taveira-Pinto, P. Rosa-Santos, Numerical modelling of the
444 ceco wave energy converter, Renewable Energy 113 (2017) 202–210.
- 445 [61] M. López, F. Taveira-Pinto, P. Rosa-Santos, Influence of the power take-
446 off characteristics on the performance of ceco wave energy converter, En-
447 ergy 120 (2017) 686–697.
- 448 [62] E. Medina-López, R. Bergillos, A. Moñino, M. Clavero, M. Ortega-
449 Sánchez, Effects of seabed morphology on oscillating water column wave
450 energy converters, Energy 135 (2017) 659–673.

- 451 [63] M. López, V. Ramos, P. Rosa-Santos, F. Taveira-Pinto, Effects of the
452 PTO inclination on the performance of the CECO wave energy converter,
453 *Marine Structures* 61 (2018) 452–466.
- 454 [64] A. Moñino, E. Medina-López, R. J. Bergillos, M. Clavero, A. Borthwick,
455 M. Ortega-Sánchez, *Thermodynamics and Morphodynamics in Wave En-*
456 *ergy*, Springer, 2018.
- 457 [65] V. Ramos, M. López, F. Taveira-Pinto, P. Rosa-Santos, Performance
458 assessment of the ceco wave energy converter: Water depth influence,
459 *Renewable Energy* 117 (2018) 341–356.
- 460 [66] E. Medina-López, A. Moñino, R. Bergillos, M. Clavero, M. Ortega-
461 Sánchez, Oscillating water column performance under the influence of
462 storm development, *Energy* 166 (2019) 765–774.
- 463 [67] O. Barambones, J. A. Cortajarena, J. M. G. de Durana, P. Alkorta, A
464 real time sliding mode control for a wave energy converter based on a wells
465 turbine, *Ocean Engineering* 163 (2018) 275–287.
- 466 [68] Z. Chao, Y. Yage, C. Aiju, Hydrodynamics research of a two-body artic-
467 ulated wave energy device, *Ocean Engineering* 148 (2018) 202–210.
- 468 [69] H.-T. Do, T.-D. Dang, K. K. Ahn, A multi-point-absorber wave-energy
469 converter for the stabilization of output power, *Ocean Engineering* 161
470 (2018) 337–349.
- 471 [70] P. Halder, M. H. Mohamed, A. Samad, Wave energy conversion: Design
472 and shape optimization, *Ocean Engineering* 150 (2018) 337–351.
- 473 [71] A. Kolios, L. F. Di Maio, L. Wang, L. Cui, Q. Sheng, Reliability assess-
474 ment of point-absorber wave energy converters, *Ocean Engineering* 163
475 (2018) 40–50.
- 476 [72] N. Sergiienko, A. Rafiee, B. Cazzolato, B. Ding, M. Arjomandi, Feasibility
477 study of the three-tether axisymmetric wave energy converter, *Ocean*
478 *Engineering* 150 (2018) 221–233.

- 479 [73] B. Wu, M. Li, R. Wu, T. Chen, Y. Zhang, Y. Ye, BBDB wave energy
480 conversion technology and perspective in China, *Ocean Engineering* 169
481 (2018) 281–291.
- 482 [74] Y. Yang, I. Diaz, M. Morales, A vertical-axis unidirectional rotor for wave
483 energy conversion, *Ocean Engineering* 160 (2018) 224–230.
- 484 [75] S. Zheng, Y. Zhang, Analytical study on wave power extraction from a
485 hybrid wave energy converter, *Ocean Engineering* 165 (2018) 252–263.
- 486 [76] G. Iglesias, H. Fernández, R. Carballo, A. Castro, F. Taveira-Pinto, The
487 wavecat©-development of a new wave energy converter, in: *World Re-*
488 *newable Energy Congress-Sweden; 8-13 May; 2011; Linköping; Sweden,*
489 57, Linköping University Electronic Press, 2011, pp. 2151–2158.
- 490 [77] H. Fernandez, G. Iglesias, R. Carballo, A. Castro, M. Sánchez, F. Taveira-
491 Pinto, Optimization of the wavecat wave energy converter, *Coastal Engi-*
492 *neering Proceedings* 1 (2012) 5.
- 493 [78] J. Abanades, D. Greaves, G. Iglesias, Wave farm impact on the beach
494 profile: A case study, *Coastal Engineering* 86 (2014) 36–44.
- 495 [79] J. Abanades, D. Greaves, G. Iglesias, Coastal defence through wave farms,
496 *Coastal Engineering* 91 (2014) 299–307.
- 497 [80] J. Abanades, D. Greaves, G. Iglesias, Coastal defence using wave farms:
498 The role of farm-to-coast distance, *Renewable Energy* 75 (2015) 572–582.
- 499 [81] J. Abanades, G. Flor-Blanco, G. Flor, G. Iglesias, Dual wave farms for
500 energy production and coastal protection, *Ocean & Coastal Management*
501 160 (2018) 18 – 29.
- 502 [82] R. J. Bergillos, A. Lopez-Ruiz, E. Medina-Lopez, A. Monino, M. Ortega-
503 Sanchez, The role of wave energy converter farms on coastal protection in
504 eroding deltas, Guadalfeo, southern Spain, *Journal of Cleaner Production*
505 171 (2018) 356–367.

- 506 [83] C. Rodríguez-Delgado, R. J. Bergillos, M. Ortega-Sánchez, G. Iglesias,
507 Protection of gravel-dominated coasts through wave farms: Layout and
508 shoreline evolution, *Science of The Total Environment* 636 (2018) 1541–
509 1552.
- 510 [84] C. Rodríguez-Delgado, R. J. Bergillos, M. Ortega-Sánchez, G. Iglesias,
511 Wave farm effects on the coast: The alongshore position, *Science of The*
512 *Total Environment* 640 (2018) 1176–1186.
- 513 [85] C. Rodríguez-Delgado, R. J. Bergillos, G. Iglesias, Dual wave energy
514 converter farms and coastline dynamics: the role of inter-device spacing,
515 *Science of The Total Environment*, 646 (2019) 1241–1252.
- 516 [86] R. J. Bergillos, C. Rodríguez-Delgado, G. Iglesias, Wave farm impacts
517 on coastal flooding under sea-level rise: a case study in southern Spain,
518 *Science of the Total Environment* 653 (2019) 1522–1531.
- 519 [87] R. J. Bergillos, M. Ortega-Sánchez, M. A. Losada, Foreshore evolution
520 of a mixed sand and gravel beach: The case of Playa Granada (Southern
521 Spain), in: *Proceedings of the 8th Coastal Sediments*, World Scientific,
522 2015.
- 523 [88] R. J. Bergillos, A. López-Ruiz, M. Ortega-Sánchez, G. Masselink, M. A.
524 Losada, Implications of delta retreat on wave propagation and longshore
525 sediment transport-Guadalejo case study (southern Spain), *Marine Geol-*
526 *ogy* 382 (2016) 1–16.
- 527 [89] R. J. Bergillos, A. López-Ruiz, D. Principal-Gómez, M. Ortega-Sánchez,
528 An integrated methodology to forecast the efficiency of nourishment
529 strategies in eroding deltas, *Science of the Total Environment* 613 (2018)
530 1175–1184.
- 531 [90] R. J. Bergillos, C. Rodríguez-Delgado, A. López-Ruiz, A. Millares,
532 M. Ortega-Sánchez, M. A. Losada, Recent human-induced coastal changes
533 in the Guadalfeo river deltaic system (southern Spain), in: *Proceedings*

- 534 of the 36th IAHR-International Association for Hydro-Environment En-
535 gineering and Research World Congress, 2015.
- 536 [91] R. J. Bergillos, C. Rodríguez-Delgado, A. Millares, M. Ortega-Sánchez,
537 M. A. Losada, Impact of river regulation on a Mediterranean delta: As-
538 sessment of managed versus unmanaged scenarios, *Water Resources Re-*
539 *search* 52 (2016) 5132–5148.
- 540 [92] R. J. Bergillos, M. Ortega-Sánchez, Assessing and mitigating the land-
541 scape effects of river damming on the Guadalfeo River delta, southern
542 Spain, *Landscape and Urban Planning* 165 (2017) 117–129.
- 543 [93] R. J. Bergillos, G. Masselink, R. T. McCall, M. Ortega-Sánchez, Modelling
544 overwash vulnerability along mixed sand-gravel coasts with XBeach-G:
545 Case study of Playa Granada, southern Spain, in: *Coastal Engineering*
546 *Proceedings*, volume 1, 2016, p. 13.
- 547 [94] M. Ortega-Sánchez, R. J. Bergillos, A. López-Ruiz, M. A. Losada, *Mor-*
548 *phodynamics of Mediterranean Mixed Sand and Gravel Coasts*, Springer,
549 2017.
- 550 [95] R. J. Bergillos, M. Ortega-Sánchez, G. Masselink, M. A. Losada, *Morpho-*
551 *sedimentary dynamics of a micro-tidal mixed sand and gravel beach, Playa*
552 *Granada, southern Spain*, *Marine Geology* 379 (2016) 28–38.
- 553 [96] J. Allen, K. Sampanis, J. Wan, D. Greaves, J. Miles, G. Iglesias, *Labora-*
554 *tory tests in the development of WaveCat*, *Sustainability* 8 (2016) 1339.
- 555 [97] J. Allen, K. Sampanis, J. Wan, J. Miles, D. Greaves, G. Iglesias, *Lab-*
556 *oratory tests and numerical modelling in the development of WaveCat*
557 (2018).
- 558 [98] R. J. Bergillos, C. Rodríguez-Delgado, M. Ortega-Sánchez, *Advances in*
559 *management tools for modeling artificial nourishments in mixed beaches*,
560 *Journal of Marine Systems* 172 (2017) 1–13.

- 561 [99] L. C. van Rijn, A simple general expression for longshore transport of
562 sand, gravel and shingle, *Coastal Engineering* 90 (2014) 23 – 39.
- 563 [100] R. Pelnard-Considère, Essai de theorie de l'évolution des formes de rivage
564 en plages de sable et de galets, *Les Energies de la Mer: Compte Rendu*
565 *Des Quatriemes Journees de L'hydraulique*, Paris 13, 14 and 15 Juin 1956;
566 Question III, rapport 1, 74-1-10 (1956).
- 567 [101] R. J. Bergillos, G. Masselink, M. Ortega-Sánchez, Coupling cross-shore
568 and longshore sediment transport to model storm response along a mixed
569 sand-gravel coast under varying wave directions, *Coastal Engineering* 129
570 (2017) 93–104.